INFLUENCE OF NON-EQUILIBRIUM CONDITIONS ON LIQUID HYDROGEN STORAGE TANK BEHAVIOR

Derek M. Machalek[1], Gabriela Bran Anleu[2], Ethan S. Hecht[3]

[1] Chemical Engineering, University of Utah, Salt Lake City, 84112, USA, derek.machalek@utah.edu
[2] Thermal/Fluid Science and Engineering, Sandia National Laboratories, P.O. Box 969, MS 9042, Livermore, 94551, USA, gabrana@sandia.gov
[3] Combustion Research Facility, Sandia National Laboratories, P.O. Box 969, MS 9052, Livermore, 94551, USA, ehecht@sandia.gov

ABSTRACT

In a liquid hydrogen storage tank, hydrogen vapor exists above the cryogenic liquid. A common modeling assumption of a liquid hydrogen tank is thermodynamic equilibrium. However, this assumption may not hold in all conditions. A non-equilibrium storage tank with a pressure relief valve and a burst disc in parallel was modeled in this work. The model includes different boiling regimes to handle scenarios with high heat transfer. The model was first validated with a scenario where normal boil-off from an unused tank was compared to experimental data. Then, four abnormal tank scenarios were explored: a loss of vacuum in the insulation layer, a high ambient temperature (to simulate an engulfing fire), a high ambient temperature with a simultaneous loss of vacuum, and high conduction through the insulation layer. The burst disc of the tank opened only in the cases with extreme heat transfer to the tank (i.e., fire with a loss of vacuum and high insulation conductivity), quickly releasing the hydrogen. In the cases with only a loss of vacuum or only external heat from fire, the pressure relief valve on the tank managed to moderate the pressure below the burst disc activation pressure. The high insulation conductivity case highlights differences between the equilibrium and non-equilibrium tank models. The mass loss from the tank through the burst disc is slower using a non-equilibrium model because mass transfer from the liquid to gas phase within the tank becomes limiting. The implications of this model and how it can be used to help inform safety codes and standards are discussed.

1. INTRODUCTION

Hydrogen has the potential to impact the transportation industry, one of the largest consumers of fossil fuel. Hydrogen fuel cell electrical vehicles (FCEVs) can provide clean and reliable transportation for long distances. In order to gain adoption, hydrogen refueling stations must be ubiquitous and safe. Extensive research has been performed to ensure the safe use of gaseous hydrogen; however, liquid hydrogen is still in its early stages of adaptation. As demand for hydrogen FCEVs increases, the hydrogen capacity of the refueling infrastructure needs to increase. Liquid hydrogen storage becomes more attractive over high pressure gaseous storage because liquid hydrogen has a higher density which allows to store larger amounts of hydrogen in smaller tanks at near ambient pressure. This makes the transportation and handling of liquid hydrogen economical and safe [1, 2]. Currently, some of the separation distances for liquid hydrogen systems specified in the hydrogen technology code from the National Fire Protection Association (NFPA 2) are conservative, and there are not enough physics based models to rigorously support reductions [3]. The separation distances are critical to hydrogen energy adoption, because the footprint of the refueling station must be large enough to be safe, but small enough that more plots of land are viable. The objective of this research is to develop a physics-based model that can be used to simulate hazardous scenarios that may be encountered in liquid hydrogen refueling stations. Specifically, a model for a liquid hydrogen storage tank is needed, so that the rate of venting and blowdown of the tank can be accurately predicted for a variety of circumstances, including normal conditions, such as boil-off, and abnormal conditions, such as a failure of the vacuum insulation.

Cryogenic tank dynamics have been previously researched for rocket fueling applications. Estey et al [4] developed a thermodynamic non-equilibrium model to characterize the blowdown process of a propellant tank, where they solve for the mass and energy equations of the liquid and vapor phase. They

assumed a massless liquid-vapor interface where heat transfer between the liquid and vapor happens only by convection. The authors in [5, 6] developed a model for the filling of a cryogenic tank and showed that heat transfer by conduction is also important when dynamic condensation blocking is present. Dynamic condensation blocking happens when heat conduction from the liquid-vapor interface to the liquid is not fast enough that the temperature of the liquid-vapor interface increases until condensation is stopped by evaporation. Petitpas [7] modified the Matlab model developed by Osipov et al. [6] to model the normal boil-off losses during transfer of liquid hydrogen from a trailer to a storage tank located at a hydrogen refueling station. The physics models the authors developed can also be used to model hydrogen releases from on-site storage hydrogen tanks at a refueling station. We build off of these previous works and present a model that also includes heat transfer via boiling, which becomes important with high heat flow into the tank. A more detailed wall heat transfer model was also included.

This work will focus on boil-offs due to heat leaks. In normal conditions, heat leaks occur due to the shape and size of the tank, as well as thermal stratification of the liquid hydrogen. As the liquid hydrogen tank sits at the hydrogen refueling station for longer times, heat transfer from the sidewalls and bottom to the liquid hydrogen occurs, increasing the temperature of the liquid hydrogen closest to the walls of the tank. The warm liquid hydrogen becomes buoyant and rises to the top of the tank. Some of the warmer hydrogen evaporates. The presence of warmer liquid hydrogen and gaseous hydrogen increases the vapor pressure in the tank [8]. This boil-off regularly vents through a pressure relief valve to ensure that the pressure inside of the tank stays within the operational limits.

The wall of the liquid hydrogen storage tank is composed of an interior steel shell, a vacuum space with multi-layer insulation (MLI) material, and an external steel shell. The vacuum and low thermal conductivity of the MLI significantly reduce the heat transfer from the outside environment [9]. Only the pressure relief valve (PRV) and burst disc are shown in Figure 1a since these two components are the ones relevant to this work. The rest of the piping and valves for loading the tank with hydrogen or discharging the hydrogen to vehicles are not shown. For safety reasons, the tank is designed to have normal boil-off flow from the vapor space in the tank through the PRV to ensure the pressure inside the tank does not increase beyond the working pressure. The PRV opens if the pressure inside the tank reaches the working pressure, and it closes once the pressure decreases below the working pressure. If the PRV malfunctions or is unable to vent sufficient vapor to maintain a pressure below the maximum allowable working pressure, the burst disc acts as a secondary safety mechanism. Burst discs generally have a larger flow area than the PRV and should be able to prevent tank rupture in the case of any abnormal circumstances. The goal of both relief devices is to decrease the pressure inside the tank and direct the hydrogen to a safe location in the event of a release.

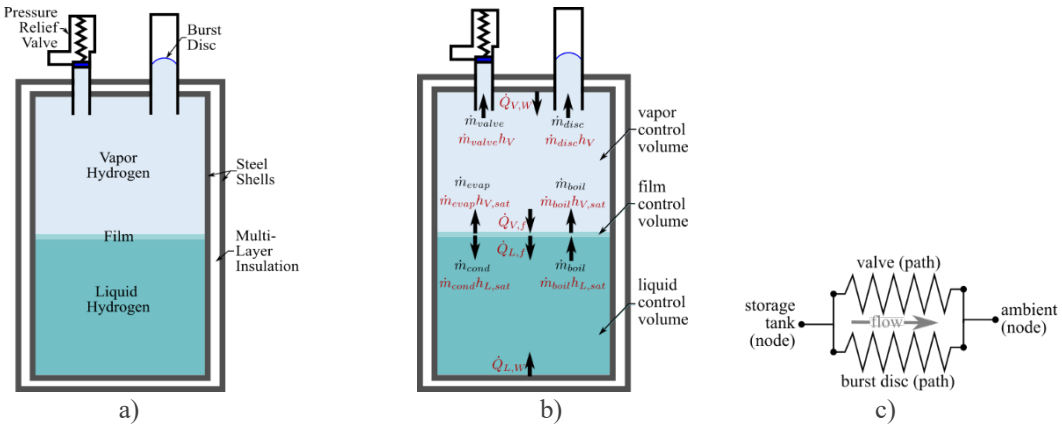

Figure 1. Diagram of a) liquid hydrogen storage tank, b) mass and energy flows in liquid and vapor control volumes (CVs) in a liquid hydrogen tank, and c) network flow modelling for a hydrogen storage tank during hydrogen releases through a valve or burst disc.

In this study, four liquid hydrogen release scenarios under abnormal conditions were investigated to demonstrate the model capabilities: 1) vacuum loss in the MLI layer, 2) an external fire engulfing the

storage tank, 3) loss of vacuum and an engulfing fire, and 4) high heat conduction through the insulation layer. The key metrics explored for the hydrogen releases are how fast hydrogen is released and whether or not the pressure relief valve is sufficient to lower the pressure of the tank to the rated tank pressure. Both thermodynamic equilibrium and non-equilibrium models of the tank were explored to determine in what scenarios the equilibrium assumption was valid and when it was not.

2. MODEL

In the equilibrium model, the liquid and gas are assumed to be in thermodynamic equilibrium (i.e., at the same temperature). That constraint allows the vapor and liquid to be treated as a single control volume with only one continuity equation. In contrast, in the non-equilibrium case the liquid and vapor will not be at the same temperature, so the liquid and vapor mass balances must be treated separately. These homogeneous volumes are separated by a thin massless film of saturated vapor as shown in Figure 1c. A detailed wall heat transfer model, which includes wall boiling for high heat transfer scenarios, was also included in the model.

The physics models were implemented in MassTran, a Sandia developed python software [10]. MassTran uses the CoolProp [11] package to calculate the properties hydrogen using a Helmholtz energy equation of state (EOS). MassTran models compressible flows in networks consisting of pressure vessels, connecting tubing, orifices, valves, and flow branches which are modeled as nodes or paths. For the equilibrium model, the tank and ambient environment are modeled as nodes, and the valve and burst disc are modeled as paths (see Figure 1b). The mass flow rates at the valve and burst disc is calculated from the momentum equation as described in [10]. For the non-equilibrium case, the tank is modeled as two nodes, one for the liquid and one for the gas. Figure 1c shows the mass (black) and energy (red) transfer between then liquid and gas node. As discussed in the theory manual [10], MassTran uses the IDA solver with adaptive timesteps from the SUNDIALS suite of differential/algebraic equation solvers [12].

2.1 Governing Equations

In the non-equilibrium tank model, the governing equations defined for the liquid phase node is different than the ones defined for the vapor phase node. The liquid mass balance is defined as,

$$\frac{dm_L}{dt} = \dot{m}_{cond} - \dot{m}_{boil} \tag{1}$$

where m_L is the mass of the liquid. The condensation rate, $\dot{m}_{cond}$, and the boiling rate, $\dot{m}_{boil}$, are described in Section 2.3 and Section 2.4. respectively. The vapor mass balance is defined as,

$$\frac{dm_V}{dt} = \dot{m}_{evap} + \dot{m}_{boil} - \dot{m}_{valve} - \dot{m}_{disc} \tag{2}$$

where m_V is the mass of the gas. The condensation and evaporation rate were assumed to be the same, but in the opposite direction ($\dot{m}_{cond} = -\dot{m}_{evap}$) and are further described in Section 2.3. The liquid energy balance is defined as,

$$\frac{dU_L}{dt} = \dot{Q}_{L,f} + \dot{Q}_{L,W} + \dot{m}_{cond} h_{L,sat} - \dot{m}_{boil} h_{L,sat} \tag{3}$$

where U_L is the internal energy of the liquid, $\dot{Q}_{L,f}$ is the heat transfer rate from the film to the liquid, and $h_{L,sat}$ is the enthalpy of the liquid phase at saturated conditions. The vapor energy balance is defined as,

$$\frac{dU_V}{dt} = \dot{Q}_{V,W} - \dot{Q}_{V,f} + \dot{m}_{boil} h_{V,sat} + \dot{m}_{evap} h_{V,sat} - (\dot{m}_{valve} + \dot{m}_{disc}) h_V \tag{4}$$

where $\dot{Q}_{V,f}$, is the heat transfer rate from the vapor to the film, and $h_{V,sat}$ is the enthalpy of the vapor phase at saturated conditions.

The equations for the equilibrium tank are simplified into a single mass and energy balance. Further, the mass and energy transfer at the interface of the two phases is computed with the thermodynamic equilibrium constraint (mass and energy transfer between the phases is instantaneous). The mass and energy balances for the equilibrium model are defined as,

$$\frac{dm}{dt} = -\dot{m}_{valve} - \dot{m}_{disc} \tag{5}$$

$$\frac{dU}{dt} = \dot{Q}_{L,W} + \dot{Q}_{V,W} - (\dot{m}_{valve} + \dot{m}_{disc})h_V \tag{6}$$

2.2 Wall Heat Transfer

The 1-D energy equation to calculate the wall temperature, T_w, along the radial coordinates, x, is described as,

$$\rho_w C_{p,w} \frac{\partial T_w}{\partial t} = \kappa_w \frac{\partial^2 T_w}{\partial x^2} \tag{7}$$

where ρ_w, $C_{p,w}$, and κ_w are the density, specific heat, and thermal conductivity of the wall, respectively. A flux is imposed at the hydrogen-wall interface ($x = 0$) and at the wall-air interface ($x = R_0$),

$$\left.\frac{\partial T_w}{\partial t}\right|_{x=0} = \frac{h_i}{\rho_w C_{p,w}} (T_w(x = 0) - T_\alpha) \tag{8}$$

$$\left.\frac{\partial T_w}{\partial t}\right|_{x=R_0} = \frac{h_{\mathrm{amb}}}{\rho_w C_{p,w}} (T_w(x = R_0) - T_{a\mathrm{mb}}) \tag{9}$$

where h_i is the convective heat transfer coefficient between the hydrogen inside the tank and the inner wall, and h_{amb} is the convective heat transfer coefficient between air and the outer wall. T_α is the temperature of phase α, and T_{amb} is the ambient temperature. R_0 is the outer radius of the steel layer.

The overall heat transfer rate, $\dot{Q}_{\alpha,W}$, between the hydrogen at phase, α, and the wall is the summation of the heat transfer rate at the curved surface (side wall, $\dot{Q}_{C,\alpha}$) and the heat transfer rate at the flat surfaces (top and bottom, $\dot{Q}_{F,\alpha}$) of the vertical tank,

$$\dot{Q}_{\alpha,W} = \dot{Q}_{C,\alpha} + \dot{Q}_{F,\alpha} = \frac{\kappa_\alpha}{f_\alpha H} \mathrm{Nu}_{C,\alpha} (f_\alpha H \pi D_h)(T_w - T_\alpha) + \frac{\kappa_\alpha}{D_h/2} \mathrm{Nu}_{F,\alpha} \left(\frac{\pi D_h^2}{4}\right)(T_w - T_\alpha) \;\; \alpha = V \; or \; L \tag{10}$$

where D_h is the tank diameter, f_α is the fraction of the height of hydrogen in phase α, and H is the overall tank height. It was assumed that the surface areas of the tank are reasonably large that the following correlations for external flow [13] can be used to calculate the Nusselt number, $\mathrm{Nu}_{\mathrm{C},\alpha}$ and $\mathrm{Nu}_{\mathrm{F},\alpha}$,

$$\mathrm{Nu}_{\mathrm{C},\alpha} = \left(0.825 + \frac{0.387 \mathrm{Ra}_{\mathrm{C},\alpha}^{1/6}}{(1 + (0.492/\mathrm{Pr}_\alpha)^{9/16})^{8/27}}\right)^2 \tag{11}$$

$$\mathrm{Nu}_{F,\alpha} = C_\alpha \mathrm{Ra}_{F,\alpha}^{n_\alpha} \text{ for } \mathrm{Ra}_{F,\alpha} < 10^9 \tag{12}$$

where Ra and Pr are the Rayleigh and Prandtl number, respectively [13] (with the tank diameter as the characteristic length for flat surfaces and $f_\alpha H$ as the characteristic length for the curved surfaces), and $C_L = 0.15$, $n_L = 1/3$, $C_V = 0.52$, and $n_V = 1/5$.

2.3 Inner-Tank Heat and Mass Transfer

In the non-equilibrium model, the state of each phase (whether superheated, subcooled, or at saturation) is based on the internal energy, and the phases are separated by a thin mass-less vapor film at the saturation temperature of the vapor phase (i.e., $T_f = T_{sat,V}$). The evaporation rate, $\dot{m}_{evap}$, and condensation rate, $\dot{m}_{cond}$, are limited by the heat transfer to the liquid-vapor interface. An energy balance on the thin vapor film can be performed to obtain the evaporation mass flow rate, $\dot{m}_{evap}$,

$$\dot{m}_{evap} = -\frac{\dot{Q}_{L,f} + \dot{Q}_{V,f}}{\Delta h_{vap}} \tag{13}$$

The heat of vaporization, $\Delta h_{vap}(T_f) = h_{V,f} - h_{L,f}$, is defined at the film temperature, T_f. The heat transfer, $\dot{Q}_\alpha$, between the film and phase α is via conduction and in some cases also via convection. While conductive heat transfer to the thin film is always happening, the only convection mechanism, natural convection, occurs in the vapor when the vapor is colder than the film or in the liquid when the liquid is hotter than the film (i.e., a higher density fluid is on top of a lower density fluid within a given phase). The heat transfer from either phase to the film is the summation of the heat transfer due to conduction, $\dot{Q}_{\alpha,cd}$, and convection, $\dot{Q}_{\alpha,cv}$, ($\dot{Q}_{\alpha,f} = \dot{Q}_{\alpha,cd} + \dot{Q}_{\alpha,cv}$). A Boundary Layer (BL) model was developed by Osipov and Muratov [5], and later modified by Petitpas [7], to account for the temperature gradients in the liquid and gas volumes. However, the simulation was highly sensitive to BL lengths, and the authors do not justify their length selection. As a result, a simpler correlation for the conductive heat transfer between the film and hydrogen in phase α is follows [14],

$$\dot{Q}_{\alpha,cd} = \left(\frac{\kappa_\alpha C_{v,\alpha} \rho_\alpha}{\pi}\right)^{1/2} A_c(T_\alpha - T_f) \tag{14}$$

The equation for natural convection is described as,

$$\dot{Q}_{\alpha,cv} = 0.156\left(\frac{g\,\beta\,\rho_\alpha^2\,(T_\alpha - T_f)}{\kappa_\alpha\,\mu_\alpha}\right)^{1/3} A_c\,(T_\alpha - T_f) \tag{15}$$

where κ_α is the thermal conductivity, $C_{v,\alpha}$ is the heat capacity, ρ_α is the density, and T_α is the temperature of the phase α (liquid or gas). T_f is the temperature of the film, A_c is the cross-sectional area of the film interface, g is the gravitational constant, β is the thermal expansion coefficient, and μ_α is the dynamic viscosity.

The state of each phase is first calculated by assuming that both phases are at the same pressure. A solver is used to find the pressure, given the internal energy of each phase as a result of the solution to the energy equations (Equations (3) and (4)), constrained by the tank volume. With the density and mass of each phase (found by solving the mass balance equations, (Equations (1) and (2)), each phase volume is calculated. The phase volumes must add up to the total tank volume ($V_V + V_L = V_{tank}$). The calculated condensation rate is adjusted when the liquid is two-phase (quality between 0 and 1). The pressure is recalculated so that the liquid is saturated (quality of 0), and the remaining tank volume is assumed to be filled with the vapor. Note that sometimes it would be preferable to assume that the vapor is saturated. However, the solver runs into issues since changing the pressure does not greatly impact liquid density. Therefore, when the liquid occupies the remaining volume after the vapor phase volume is set, the liquid has drastic changed in volume and as a result, it has unreasonable properties (e.g., very high temperature).

After this calculation, the vapor phase may be two-phase (quality between 0 and 1). This sometimes occurs when the pressure is recalculated if the liquid phase density (at saturation) is low enough to expand and confine the vapor phase into a small volume. In this case, an additional condensation mass,

$m_{cond,add}$, is used to adjust the density of the liquid and vapor, and it is calculated using the quality of the vapor, χ_V, and the m_V the mass of the vapor,

$$m_{cond,add} = (1 - \chi_V)m_V \tag{16}$$

2.4 Boiling

When the liquid becomes saturated and the temperature difference, ΔT , between the wall and the liquid is large enough, pool boiling will occur. This is a secondary form of heat and mass transfer between the liquid and vapor phases. There are four regimes of pool boiling. Table 1 shows the temperature difference and heat transfer function for each of those regimes as well as the critical heat flux (CHF) and minimum heat flux (MHF) [15]. Before boiling was added to the model, in high heat transfer scenarios the liquid in the tank became very hot because the liquid absorbed heat from the wall quickly, but the evaporation rate and associated energy loss through the film was low. By adding boiling to the model, the rapid evaporation rate is captured. The boiling rate, $\dot{m}_{boil}$, is calculated by dividing the heat transfer due to boiling by the heat of vaporization, since the liquid is saturated,

$$\dot{m}_{boil} = \frac{\dot{q}_{boil} A_{s,L}}{h_{vap}} \tag{17}$$

where $A_{s,L}$ is the surface area of the liquid to wall interface.

Table 1. Hydrogen boiling regimes [15].

Regime	ΔT (K)	$\dot{q}_{boil}(\mathrm{W/m^2})$
Convective	0-0.1	$0.16\mathrm{Ra}^{1/3}\Delta T$
Nucleate boiling	0.1-3	$6309\Delta T^{2.52}$
Critical heat flux	3	$(0.18 - 0.14(P/P_C)^{5.68})h_{vap}\rho_V\left(\frac{g\sigma(\rho_L - \rho_V)}{\rho_V^2}\right)^{1/4}$
Transition	3-15	$\dot{Q}_{CHF} - \frac{\Delta T - \Delta T_{CHF}}{\Delta T - \Delta T_{MHF}}(\dot{Q}_{CHF} - \dot{Q}_{MHF})$
Minimum heat flux	15	$0.31h_{vap}\rho_V\left(\frac{g\sigma(\rho_L - \rho_V)}{(\rho_L + \rho_V)^2}\right)^{1/4}$
Film boiling	>15	$f(D, \rho, g, \kappa, \Delta T)$ (not included in this model)

The film boiling regime was not implemented in the code because the temperature difference between the wall and the hydrogen is not expected to be larger than 15 K, even in abnormal heat transfer cases. The expression for the film boiling critical heat flux can be found in [15].

3. RESULTS AND DISCUSSION

In this section, a typical dormant liquid hydrogen tank is first studied and used to validate the model. Then, four abnormal tank pressure relief scenarios are explored: 1) vacuum loss in the MLI, 2) an external fire engulfing the storage tank, 3) loss of vacuum and an engulfing fire, and 4) high conduction through the insulation layer. The key metrics for these hydrogen releases are how fast hydrogen is released and whether or not the pressure relief valve is sufficient to lower the pressure of the tank to the rated tank pressure. It was assumed that the pressure relief valve opens at 3.1 bar and reseals when the tank pressure drops to 2.9 bar, and that the burst disc opens at a hydrogen vapor pressure of 4 bar, and it does not close again.

3.1 Validation

The hydrogen storage tank simulations were run with the specifications of a cylindrical hydrogen storage tank located at Lawrence Livermore National Laboratory. Experimental results from the tank were available for validation of the simulations [7]. Table 2 and Table 3 show the geometry specifications and the thermal properties of the hydrogen storage tank used in the simulations. The thermal properties

of the wall materials were assumed constant. The thermal properties of the inner steel layer were evaluated at 20 K, while the properties of the outer steel layer were evaluated at 300 K. The effective specific heat and bulk density of MLI in vacuum space were assumed to be very low values, and the effective thermal conductivity was estimated to be 20.0×10^{-5} W/m-k [16]. These properties were adjusted for the case where the vacuum is lost, and air fills the space where the MLI is located.

Table 2. Tank geometry.

Parameter	Value
Tank diameter (m)	2
Tank height (m)	3.97
Safety valve diameter (m)	0.005
Burst disc diameter (m)	0.038

Table 3. Thermal properties of the hydrogen storage tank

Parameter	Inner steel wall	Outer steel wall	MLI (with vacuum)	MLI (no vacuum)
Thickness (m)	0.0111	0.0038	0.0508	0.0508
Specific heat, C_p (J/kg-K)	25	450	0.1	1000
Conductivity, κ (W/m-K)	3	15	20.0×10^{-5}	0.022
Density, ρ (kg/m3)	8050	8050	0.1	1.225

For validation, the tank described by [7] with normal boil-off was simulated. As the liquid hydrogen tank sits unused, the liquid hydrogen starts slowly heating up until the vapor pressure inside the tank reaches 3.1 bar. At this point, the pressure relief valve opens to lower the pressure inside of the tank to 2.9 bar. Once the tank reaches a pressure of 2.9 bar, the pressure relief valve closes. Numerically, these paths within MassTran (see Figure 1b) are controlled with state events that track if a pressure triggering event has occurred, which causes the path to open or close.

Figure 2 shows the experimental and numerical volume fraction of liquid in the tank. The equilibrium tank model results are shown here because of computation efficiency for simulating the entire discharge, and because the long timescale mass loss is the same as the non-equilibrium model (discussed later) for slow tank heat transfer.

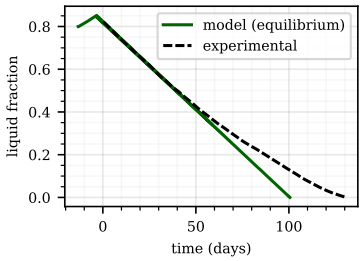

Figure 2. Comparison of model to experimental [7] hydrogen release.

Since the simulation models the case of freshly loaded hydrogen to the storage tank, there is a temporal difference with the experimental data. In the model, the hydrogen first heats up, expands, pressurizes (increasing the liquid fraction) and begins to vent at 3.1 bar (over the course of about 10 days). The liquid fraction in the tank then begins to decrease, and it aligns with the experimental data after approximately 13.5 days (zero days on the abscissa). The experimental loss of hydrogen from the storage tank is approximately the same as the simulation for the next 50 days of venting. However, after that point the venting in the experimental tank starts to slow down, while the simulation continues to decrease at the same rate, with the tank emptying 30 days after the simulation projects. The heat transfer to the tank, which drives pressurization and mass transfer out of the tank, appears to be a function of the liquid volume, which is not captured by the model.

Figure 3a shows the tank conditions for the non-equilibrium and the equilibrium models with normal heat transfer. The top frame of Figure 3a zooms in on the first 30 days of hydrogen mass loss from the tank for the equilibrium and non-equilibrium models during this normal boil-off process. The pressure relief valve will safely handle the hydrogen release. Over the course of many releases, the equilibrium and non-equilibrium models are approximately the same. However, each pressure relief episode in the non-equilibrium case releases approximately 0.25 kg of hydrogen, while in the equilibrium model, over 4 kg are released. In Figure 3a, both the equilibrium and non-equilibrium models predict the hydrogen in the tank to heat up at a similar rate, as illustrated by the time to start venting.

The major difference between the two models is how the venting cycles happen. For the equilibrium model, when the vapor pressure drops from opening the pressure relief valve, some of the liquid phase immediately evaporates to preserve thermodynamic equilibrium. As a result, the pressure in the tank does not drop as fast, and more vapor leaves the tank before the 2.9 bar threshold to close the valve is reached. On the other hand, in the non-equilibrium case, when the vapor phase leaves the tank through the pressure relief valve and the vapor pressure drops, the dynamics of mass transfer becomes critical. The evaporation due to heat transfer through the MLI is not as fast as the instantaneous evaporation with the thermodynamic equilibrium model and as a result the vapor pressure drops to 2.9 bar quickly. However, since less energy is lost in each venting episode, less energy is required to pressurize the tank back to 3.1 bar and re-open the vent. This is also shown in the rapid temperature and pressure cycles in the tank for the non-equilibrium model in the bottom two frames of Figure 3a. In the non-equilibrium model, the liquid temperature is stable compared to the vapor temperature. The higher liquid temperature in the non-equilibrium case, compared to the equilibrium case, causes faster heat transfer to the vapor and faster pressurization.

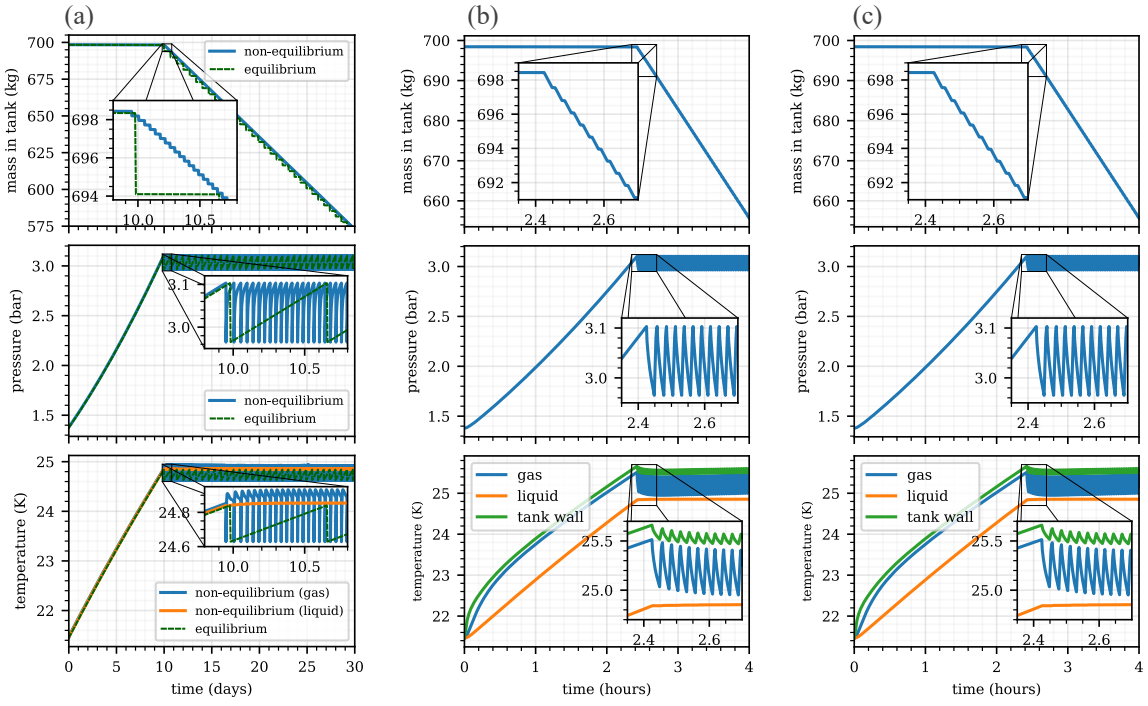

Figure 3. Tank mass, pressure, and temperature for the case of a) non-equilibrium and equilibrium models with normal heat transfer, b) loss of vacuum in the insulation layer, and c) an external fire (ambient temperature of 1200 K).

3.2 Loss of Vacuum

One quasi-real-world scenario that these tanks may encounter is loss of vacuum in the insulation layer between the steel shells. In this scenario, the gap between the two steel shells is assumed to be filled

with air (we neglect the physical layers of insulation), so the thermal conductivity, density, and heat capacity of air (see Table 3) are used for the insulation layer.

Figure 3b shows that the pressure relief valve can safely reduce the tank pressure below 2.9 bar for the non-equilibrium model. With the loss of vacuum, the pressure relief valve begins to vent after approximately 2.4 hours and vents about 35 times an hour, compared to the normal heat transfer case where it starts to vent after nearly 10 days and at a frequency on the order of 1 time every hour. The rapid cycling of the valve may lead to failure. The temperature of the liquid, vapor, and inside wall of the tank is shown in the bottom frame of Figure 3b. The gas and wall temperatures both oscillate slightly as the relief valve opens and closes. The temperature difference between the liquid and wall ranges from about 0.6-0.7 K. This results in nucleate boiling (see Table 1) increasing the mass transfer from the liquid to the gas.

The mass loss from the tank is shown in the top frame of Figure 3b. If the pressure relief functions properly, it can safely reduce the pressure of the tank. The tank will release hydrogen continuously for about 25 hours at an average rate of 27 kg/h. Each venting episode releases about 0.7 kg of hydrogen vapor.

3.3 Engulfing Fire

A second quasi-real-world scenario that was explored was high external temperatures to the tank, as might be experienced if there were an external fire. The scenario considers the case where the ambient temperature around the hydrogen storage tank is 1200 K, a high estimate (i.e. worst case) for the temperature reached in a bonfire test [17]. Only convective heat transfer is considered, no radiation from the fire, and the entire ambient surroundings are at this temperature, not just one side of the tank. Only the non-equilibrium model is considered.

The plots for the case of the external fire, shown in Figure 3c, are similar to the loss of vacuum in the insulation, although the release is a bit slower in this case. The middle frame of Figure 3c shows the pressure variation with the rapid opening and closing of the safety relief valve. The valve opens and closes about 6 times per hour, as compared to about 35 releases per hour in the loss of vacuum case (Figure 3b). The bottom frame of Figure 3c shows the temperature cycling with the valve opening and closing. The heat transfer through the wall is relatively slow because the vacuum insulation is intact. As a result, the liquid and wall temperatures remain within 0.2 K of each other. While this temperature difference is less than the loss of vacuum, it still results in some nucleate boiling.

The mass loss of hydrogen from the tank is shown in the top frame of Figure 3c. The mass loss from the tank is managed with the pressure relief valve. The average venting rate is 1.1 kg/h, which would require about 636 hours of venting to remove the hydrogen. Each venting episode release about 0.25 kg of gaseous hydrogen.

3.4 Engulfing Fire with Loss of Vacuum

The third examined case is the combination of the previous two cases, an external fire with loss of vacuum in the insulation layer. In other words, the ambient temperature is set to 1200 K, and the thermal conductivity, density, and heat capacity of air (see Table 3) were used in the middle layer of the wall. This case could happen if an external fire damages the tank causing it to lose vacuum in the wall.

Figure 4a illustrates the details of what happens in the tank. As the tank heats up and pressurizes to 3.1 bar, the pressure relief valve opens, after 35 minutes. While this reduces the rate of pressurization, it does not reduce the pressure and the tank continues to pressurize to 4 bar, while still releasing mass. The pressure relief valve cannot handle this case. After the burst disc opens, the tank rapidly releases hydrogen until the vapor phase is at the pressure of the ambient environment. Then the tank continues to lose mass at a lower rate through the bust disc until it is empty. During pressurization, the tank wall is about 2.5 K hotter than the liquid in the tank. This is still in the nucleate boiling regime. After the

burst disc opens, the mass loss is limited by the heat transfer through the wall; the vaporization rate of liquid hydrogen, driven by nucleate boiling is relatively fast.

The mass loss for this scenario is shown in the top frame of Figure 4a. The initial hydrogen release rate is about 0.7 kg/min when the pressure relief valve opens. When the burst disc opens, the hydrogen release is about 60 kg/min for 9 seconds as the vapor space pressure returns to ambient, then it settles to a steady release rate of 2.7 kg/min, limited by the energy transfer through the wall.

3.5 High conduction through the insulation layer

To push the model limits and elucidate other phenomena, a case with abnormally high conduction through the insulation layer is explored. In this scenario, the insulation thermal conductivity is set to 1 W/m-K. This thermal conductivity is between the value for air (0.022 W/m-K) and aluminum (205 W/m-K), yielding a low but realistic heat transfer resistance through the wall (e.g., for a tank with a different geometry and/or insulation material). Similar to the case of normal heat transfer to the tank, both the equilibrium and non-equilibrium models show a similar pressure increase and both models predict the start of venting at the same time (see Figure 4b).

Interestingly, the bottom frame of Figure 4b shows how the vapor and liquid in the non-equilibrium tank are at significantly different temperatures. Since the vapor phases for both the equilibrium and non-equilibrium cases are at approximately the same pressure, the colder, non-equilibrium gas, will have a lower density and therefore must have a smaller gaseous fraction of the tank to have the same pressure. The temperature difference between the wall and the liquid for the non-equilibrium model is approximately 5-11 K, depending on the point in the release, which is firmly in the transition boiling regime. This increases the mass flux from the liquid to vapor phase, but not to the same rate as the equilibrium model, since there are still differences in the tank behavior.

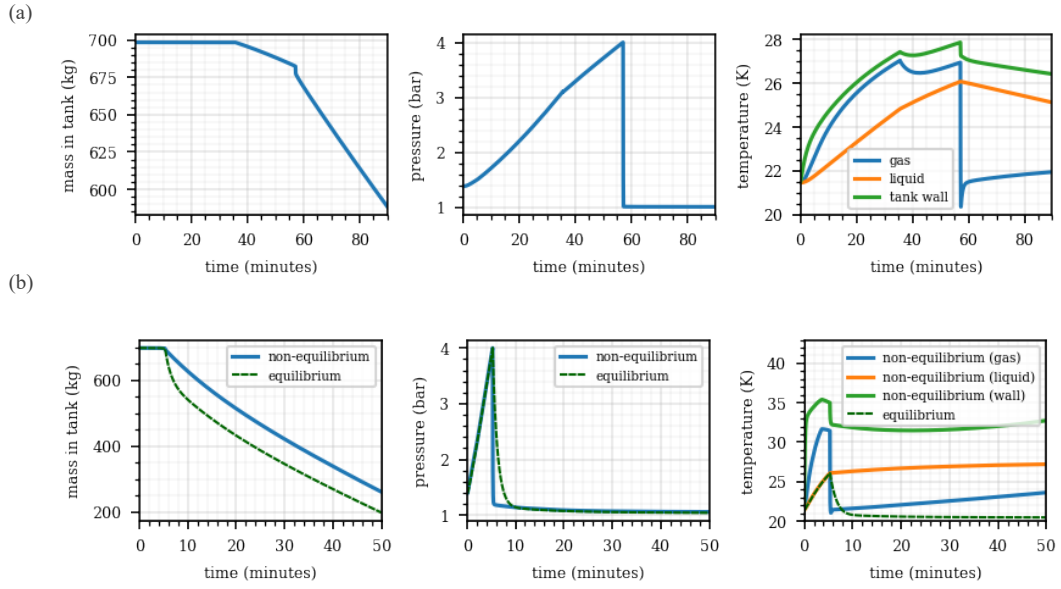

Figure 4. a) Tank mass, pressure, and temperature for the case of a) an engulfing fire with a loss of vacuum in the insulation layer, and b) tank mass, pressure, and temperature for the case of increased conduction through the insulation layer ($\kappa_{insulation}$ = 1 W/m-K).

The pressure relief valve opens at 3.1 bar but does not have a noticeable impact on depressurizing the tank (see Figure 4b). The pressure relief valve opening causes the equilibrium gas temperature to decrease slightly, prior to the burst disc opening (3-5 minutes). Flow through the valve removes energy from the vapor phase, causing the temperature to drop, but the mass flow rate is not able to control the pressure rise. Instead, the tank pressure rises to 4 bar and the burst disc opens. In the equilibrium model, the pressure drop is slower (due to the instantaneous evaporation from liquid to gas), with a more

dramatic initial loss of mass. In the non-equilibrium model, the vapor phase loses pressure very quickly. The mass loss is then limited by evaporation and boiling from the liquid phase. Finally, both the equilibrium and non-equilibrium models reach a state where the mass loss is limited by heat transfer through the tank, at around 10 minutes, where the pressure in both models is around atmospheric and the mass loss rate is the same for both models.

The mass loss from this tank is illustrated in the top frame of Figure 4b. The mass is lost from the tank over the span of about an hour. After the burst disc opens, in the non-equilibrium case, the first 100 kg are vented from the tank in about 6 minutes, while the equilibrium model predicts this mass loss to occur in under a minute. After this initial high rate of venting, both releases eventually settle to a mass loss rate of about 9 kg/min.

4. CONCLUSIONS AND FUTURE WORK

Five release scenarios for a liquid hydrogen storage tank were examined. First, a validation scenario with normal boil-off was compared to experimental data from a real-world liquid hydrogen tank. Then, four abnormal scenarios were explored: 1) the loss of vacuum in the insulation layer, 2) a high ambient temperature (engulfing fire), 3) a high ambient temperature with loss of vacuum, and 4) high conduction through the insulation layer. Only the cases with extreme heat transfer to the tank, cases 3 and 4, cause the burst disc of the hydrogen tank to open and release hydrogen quickly (30-60 kg/min). In the case of loss of vacuum or external heat from a fire, cases 1 and 2, the pressure relief on the tank is sufficient to keep the pressure in the tank below operational upper limits. The result was a controlled release of hydrogen from the tank, but at a much faster rate than the normal heat transfer. For the release through the pressure relief valve, the equilibrium model is sufficient to model the blowdown. However, when only a single venting event is of interest or abnormal heat transfer occurs (e.g., due to fire and/or vacuum loss), the equilibrium model is not able to capture the behavior. In those cases, the mass transfer between the liquid and vapor phase (evaporation and boiling) become critical.

The model could be exercised for other tank volumes or geometries (e.g., horizontal tanks). The results from this work can be taken a step further to model flames or hydrogen mass transfer to help set safety codes and standards for hydrogen storage tanks, helping to reduce the footprint of the liquid hydrogen fueling stations while maintaining safety.

The experimental release of hydrogen from the storage tanks decreases with tank volume. However, the presented model has a constant release of hydrogen regardless of tank fill. Since the mass loss in the tank is so closely tied to heat transfer, it is likely that the heat transfer through the tank depends on the height of liquid in the tank. One possible explanation is that the MLI properties are impacted by the height of liquid in the tank. Another explanation is that the model does not consider 2-D gradients in temperature (either the fluid or the wall), which may cause differences in heat transfer through the tank.

Other potential improvements to the model include the use of subcooled vapor or superheated liquid states. This would require a departure from CoolProp. Temperature dependent wall properties (C_p and κ) may improve accuracy. Finally, adding spatial discretization to the vapor and liquid would add granularity to the simulation, and it would better predict the thermal stratification that is known to exist in these liquid hydrogen tanks. The current 0-D model assumes instantaneous mixing of the hydrogen. As a result, when boiling occurs in the model ($T_w - T_L > 0.1$), rapid heat transfer happens in part because the heat transfer rate through the liquid is assumed to be instantaneous. In other words, the current boiling heat transfer model overestimates the heat transfer from the wall to the liquid. A correction factor or maximum heat transfer rate could be considered since the cooler liquid at the middle of the liquid phase needs time to reach the wall. Instead of boiling, the system could also be modeled as flash evaporation, like the work of Tani et al. [18].

Experiments to precisely determine the mass transfer mechanism between the liquid and vapor phase would help validate the model further. In the hazardous release scenarios, the heat transfer between the liquid and vapor phases is critical to keep the hydrogen from releasing as much hydrogen as predicted

by the non-equilibrium model. In order to assist in the validation and elucidation of these mechanisms, detailed specifications of the tank are needed.

ACKNOWLEDGMENTS

The U.S. Department of Energy's (DOE) office of Energy Efficiency and Renewable Energy's (EERE) Hydrogen and Fuel Cell Technologies Office (HFTO) supports the development of science-based codes and standards through the Safety, Codes and Standards program sub-element. The authors gratefully acknowledge funding from HFTO and the support of subprogram manager Laura Hill for this work.

Sandia National Laboratories is a multi-mission laboratory managed and operated by National Technology and Engineering Solutions of Sandia LLC, a wholly owned subsidiary of Honeywell International Inc. for the U.S. Department of Energy's National Nuclear Security Administration under contract DE-NA0003525. This paper describes objective technical results and analysis. Any subjective views or opinions that might be expressed in the paper do not necessarily represent the views of the U.S. Department of Energy or the United States Government.

REFERENCES

1. Barthélémy, H., *Hydrogen storage–Industrial prospectives.* International journal of hydrogen energy, 2012. **37**(22): p. 17364-17372.
2. Wolf, J., *Liquid hydrogen technology for vehicles.* Handbook of fuel cells, 2010.
3. NFPA, *NFPA 2 Hydrogen Technologies Code*. 2020, NFPA.
4. Estey, P.N., D.H. Lewis Jr, and M. Connor, *Prediction of a propellant tank pressure history using state space methods.* Journal of Spacecraft and Rockets, 1983. **20**(1): p. 49-54.
5. Osipov, V. and C. Muratov, *Dynamic condensation blocking in cryogenic refueling.* Applied Physics Letters, 2008. **93**(22): p. 224105.
6. Osipov, V.V., et al., *Dynamical model of rocket propellant loading with liquid hydrogen.* Journal of Spacecraft and Rockets, 2011. **48**(6): p. 987-998.
7. Petitpas, G., *Simulation of boil-off losses during transfer at a LH2 based hydrogen refueling station.* International Journal of Hydrogen Energy, 2018. **43**(46): p. 21451-21463.
8. Sherif, S., N. Zeytinoglu, and T. Veziroğlu, *Liquid hydrogen: potential, problems, and a proposed research program.* International journal of hydrogen energy, 1997. **22**(7): p. 683-688.
9. Hedayat, A., et al. *Variable density multilayer insulation for cryogenic storage*. in *36th AIAA/ASME/SAE/ASEE Joint Propulsion Conference and Exhibit*. 2000.
10. Bozinoski, R., *MassTran (v0.19.1) Theory Guide*. 2019.
11. Bell, I.H.a.W., Jorrit and Quoilin, Sylvain and Lemort, Vincent, *Pure and Pseudo-pure Fluid Thermophysical Property Evaluation and the Open-Source Thermophysical Property Library CoolProp.* Industrial and Engineering Chemistry Research, 2014. **53**(6): p. 2498-2508.
12. Hindmarsh, A.C., et al., *SUNDIALS: Suite of nonlinear and differential/algebraic equation solvers.* ACM Transactions on Mathematical Software (TOMS), 2005. **31**(3): p. 363-396.
13. Incropera, F.P., et al., *Principles of heat and mass transfer*. 2013: Wiley.
14. Daigle, M., M. Foygel, and V. Smelyanskiy. *Model-based diagnostics for propellant loading systems*. in *2011 Aerospace Conference*. 2011. IEEE.
15. Wang, L., et al., *Correlations for calculating heat transfer of hydrogen pool boiling.* International Journal of Hydrogen Energy, 2016. **41**(38): p. 17118-17131.
16. Sutheesh, P. and A. Chollackal. *Thermal performance of multilayer insulation: a review*. in *IOP Conference Series: Materials Science and Engineering*. 2018. IOP Publishing.
17. Zheng, J., et al., *Heat transfer analysis of high-pressure hydrogen storage tanks subjected to localized fire.* International journal of hydrogen energy, 2012. **37**(17): p. 13125-13131.
18. Tani, K., et al., *Prediction of pressure reduction rate in 30 m3 liquid hydrogen tank based on experimental and numerical analysis.* 2019.